Indonesian Journal of Science & Technology

Journal homepage: http://ejournal.upi.edu/index.php/ijost/

Effects of Heat Input and Preheating Temperature on the Microstructure and Hardness of Repairing the Heat-Affected Zone of Thermite Welded Rail Head Surface

Prapas Muangjunburee [1], Hein Zaw Oo[1], Shayfull Zamree Abd Rahim[2], Buntoeng Srikarun[3,]*

[1]Prince of Songkla University, Hat Yai, Songkhla, Thailand
[2]Universiti Malaysia Perlis (UniMAP), Arau, Perlis, Malaysia
[3]Walailak University, Nakhon Si Thammarat, Thailand
*Correspondence E-mail: buntoeng060@gmail.com

ABSTRACT

The heat-affected zone (HAZ) of a thermite weld contains softer parts that are weak and need to be modified for best rail performance. This study examines how welding heat inputs of FCAW, and preheating temperatures affect the microstructure and hardness of its weld metal and HAZ after repairing the weak area of thermite welded rail. To improve the weak area's microstructure and hardness without degrading the original thermite-welded rail, a groove was carved from the center of the HAZ on the rail head and filled using flux-cored arc welding. The investigation used two welding currents and preheating temperatures referred to as FCAW 1 and FCAW 2. The optical and electron microscopic characterization of the pearlite microstructure and interlamellar spacing were carried out. Additionally, micro-Vickers hardness testing is done. The typical hardness of the HAZ in FCAW 1 was 410 HV, whereas, in FCAW 2, it was 340 HV. The interlamellar spacings of HAZ in FCAW 1 and FCAW 2 are 80 and 105 nm, respectively. The faster cooling made pearlite interlamellar spacing finer. The decrease in lamellar spacing leads to an increase in hardness. For thermite welded rail head surface HAZ repair, greater heat input and preheating temperature with slow cooling rate work.

ARTICLE INFO

Article History:
Submitted/Received 21 Feb 2024
First Revised 01 Apr 2024
Accepted 16 Jun 2024
First Available online 18 Jun 2024
Publication Date 01 Sep 2024

Keyword:
Interlamellar spacing,
Pearlite,
Rail,
Repair weld,
Thermite welding.

1. INTRODUCTION

Railway steels are manufactured with exact specifications and joined together to provide a continuous structure for railway systems. In the context of the railway infrastructure, it is essential to investigate the characteristics of rail-welded sections (Bonniot *et al.*, 2018; Jiang *et al.*, 2017). In recent times, there has been a significant change in the method used for joining railway tracks, since the traditional method of employing plates for bolting has been replaced. However, it is generally observed that bolted joints exhibit higher maintenance expenses and are susceptible to failure at the joints. Continuous welded rail is utilized for several significant reasons, with the primary objective being the reduction of maintenance costs (Skyttebol *et al.*, 2005). The installation of continuously welded rails results in a smooth surface in comparison to rail junctions that are fastened with bolts. It allows the train to pass more efficiently and reduces any unwanted vibrations and noises (Hauser, 1978). The safety and stability of a continuous rail system depend mainly on the quality of the welded joint between rails (Lesage *et al.*, 2023). Welded rail sections have different microstructures and mechanical properties than rail steel. Thus, damage to the welded rail and damage to the original rail are different (Kendall *et al.*, 2022).

Thermite welding is one of the most employed processes to install new rails and repair broken rails around the world (Yuan *et al.*, 2010; Saita *et al.*, 2013). Thermite welding is a recognized technique in field operations due to several factors (Kewalramani *et al.*, 2023). These include the reasonable cost of equipment and consumables, a simple setup process, no disruption to routine railway operations, the portability of equipment, and the ability to weld many rails (Ilić *et al.*, 1999; Schroeder & Poirier, 1984). The rail weld joint quality is affected by a significant component, namely the reduced hardness observed in the softening zones. These zones are present at the end of the heat-affected zone (HAZ) close to the base rail (Weingrill *et al.*, 2019).

The primary damage originates mainly from the alterations in the metallurgical and mechanical characteristics of the HAZs (Su *et al.*, 2020). The most common microstructure observed in rail steel utilized in global railway industries is mostly pearlite microstructure. This is attributed to its high strength, good wear resistance, and cost-effective manufacturing (Tressia *et al.*, 2020). One of the primary challenges associated with thermite welding relates to the undesired spheroidization of pearlite and the subsequent decrease in hardness observed inside the HAZ region (Liu *et al.*, 2021). Numerous investigations have provided evidence supporting the presence of reduced hardness and the formation of a spheroidized microstructure inside the HAZ of thermite-welded rails (Kozyrev *et al.*, 2020; Li *et al.*, 2011; Merıç *et al.*, 2002). The hardness value of the HAZs is shown to be lower than that of the rail steel, which can result in significant localized plastic deformation and battering (Su *et al.*, 2020). In the past, rail grinding was used to remove the batter. Weld batter cannot be controlled specifically by rail grinding (Mutton & Alvarez, 2004). As a result, it is important to explore another option for enhancing the soft region at the HAZ of thermite welds.

To minimize plastic deformation, commonly referred to as batter, occurring on the running surface of the rail in the HAZ of a thermite weld, Hernández et al. (2016) employed laser cladding. Nevertheless, a significant challenge in laser cladding is the presence of martensite phases. This study demonstrates the effective improvement of the HAZ in thermite welds using laser cladding technique accompanied by controlled heat treatments. Due to its high price and limited applicability in the field, laser cladding is difficult to select. Hence, it is necessary to determine and evaluate an affordable welding technique.

DOI: https://doi.org/10.17509/ijost.v9i2.71238
p-ISSN 2528-1410 e-ISSN 2527-8045

Flux-core arc welding (FCAW) is a commonly used welding technique for the maintenance of damaged rails (Dahl *et al.*, 1995). FCAW mainly utilizes flux-cored wire electrodes rather than solid wire electrodes. Several researchers have conducted studies on the repair of running surface rails using gas metal arc welding and flux-cored arc welding methods (Grossoni *et al.*, 2021; Allie *et al.*, 2011a; Aglan *et al.*, 2013; Allie *et al.*, 2011b). Previous investigations focused exclusively on the repair of damaged rails.

A potential issue of thermite rail welding is the occurrence of surface defects on the welded rails before the joint's expected endurance. In the industry of railway infrastructure, this problem has existed for a very long time. Over a long period of application, thermite-welded rails may undergo the formation of surface defects. One limitation of thermite rail welding, which adversely affects the endurance and strength of the weld, is the formation of cementite spheroidization and the subsequent reduction in hardness observed in the HAZ of the thermite weld. To effectively handle this problem on the service rails, it is imperative that the methods used are both easy and efficient.

Moreover, a groove on the worn thermite weld surface of operational rails is simple to create. Flux-cored arc welding is highly practical for field sites due to its ability to utilize the same power source as MMA welding. There is no need for expensive procedures or equipment to repair the damaged surface on the thermite weld at the railway site. The parameters and results obtained from this study provide the potential for fast and cost-effective implementation in the actual railway engineering industry. This study aims to repair the soft zone at the inter-critical HAZ of thermite-welded rails using FCAW, variable welding heat inputs, and preheating temperatures. This study also examines how welding heat inputs and preheating temperatures affect the microstructure and hardness of FCAW weld metal and its HAZ.

2. METHODS

2.1. Experimental Procedures

The R260 rail steel type was joined together using the thermite welding process. Thermite welding was performed with an Australian Thermit welding set. Flux-cored arc welding (FCAW) with a 1.6 mm pearlitic wire electrode was used to fill a slot that was 10 mm in diameter and 5 mm in depth made at the thermite weld's HAZs (see **Figure 1**). The quantitative analysis of chemical composition for as-received R260 rail and thermite weld was examined using a Thermo ARL Model 3460 optical emission spectroscopy (OES). **Table 1** provides the chemical composition of the welding electrode, thermite weld, and rail steel. The chemical composition of the FCAW electrode was from the manufacturer. An OES technique was employed to analyze the chemical composition of rail steel and thermite welds. Welding voltage, travel speed, and electrode polarity were 25 V, 45 cm/min, and direct current electrode positive (DCEP) for both conditions. A flow rate of 20 l/min was maintained using pure CO_2 gas as a shielding gas.

This study compares two welding conditions with varying currents and preheating temperatures. Throughout the paper, the first condition will be referred to as FCAW 1 and the second as FCAW 2. FCAW 1 used a welding current of 200 A and a preheating temperature of 350°C, whereas FCAW 2 used a welding current of 250 A and a preheating temperature of 500°C. The heat input of FCAW 1 and FCAW 2 was 6.7 kJ/cm and 8.3 kJ/cm, respectively. To perform welding on railway steel, it is necessary to subject it to a preheating process at a temperature of 350°C, as determined by the carbon equivalent calculation outlined in equation 1 (Alhassan & Bashiru, 2021), resulting in a carbon equivalent value of 0.94%. The FCAW 2 sample was wrapped with a ceramic wool blanket after welding to keep up the

DOI: https://doi.org/10.17509/ijost.v9i2.71238
p-ISSN 2528-1410 e-ISSN 2527-8045

cooling rate, but the FCAW 1 sample was not. **Figure 2** displays a flowchart outlining the concise experimental procedures for two different conditions.

$$\text{Carbon equivalent (\%)} = C + \frac{1}{6}Mn + \frac{1}{24}Si + \frac{1}{5}Cr + \frac{1}{4}Mo + \frac{1}{15}Ni \quad (1)$$

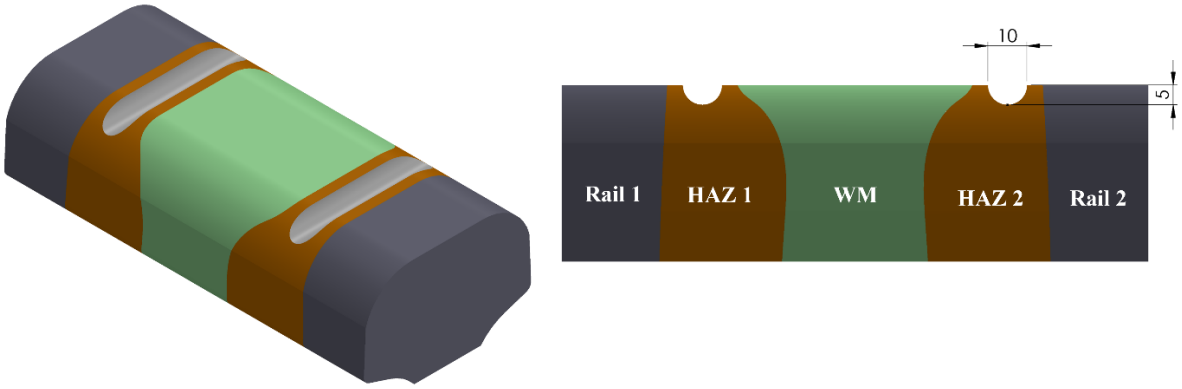

Figure 1. Schematic of groove location to repair thermite HAZ.

Table 1. Chemical composition of FCAW electrode, rail steel, and thermite weld metal.

Elements	C	Si	S	Mn	Cr	P	Ni	Mo	V	Cu	Al	Fe
FCAW Electrode	0.13	0.64	-	1.7	0.48	-	-	0.53	-	-	-	Rest
Rail Steel	0.78	0.31	0.01	0.75	0.04	0.1	-	-	-	-	-	Rest
Thermite Weld	0.54	0.67	0.007	1.05	0.18	-	0.07	0.03	0.09	0.03	0.16	Rest

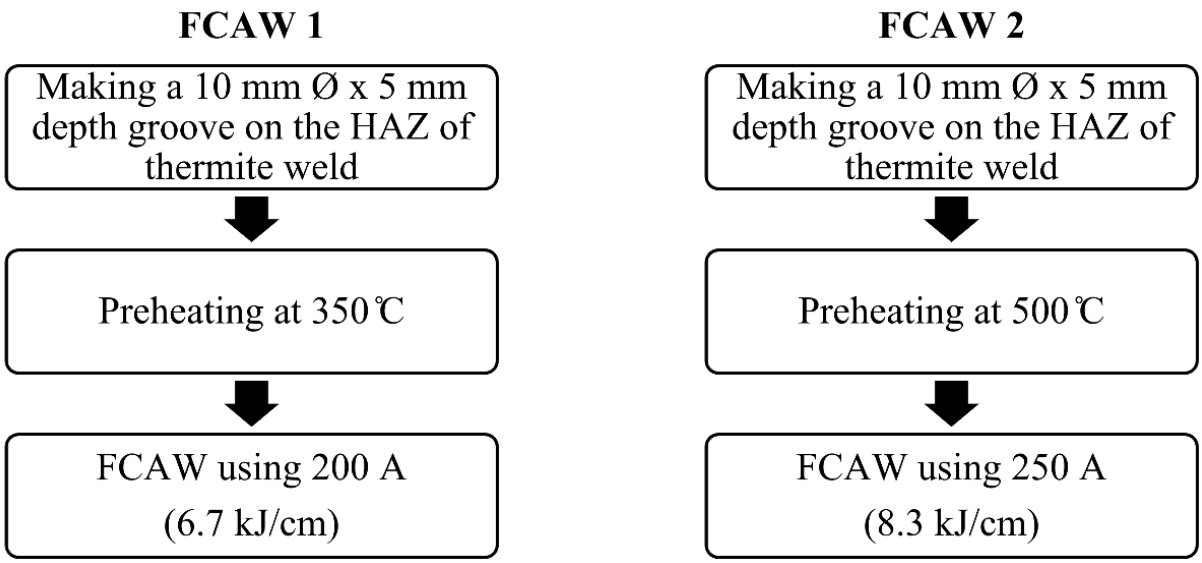

Figure 2. Schematic brief experimental procedures.

DOI: https://doi.org/10.17509/ijost.v9i2.71238
p-ISSN 2528-1410 e-ISSN 2527-8045

2.2. Metallographic Analysis

The macrostructure of the repaired HAZ of thermite weld on the rail head surface using FCAW welding was cross-sectionally analyzed using an Olympus SZ2-ET stereo camera. An optical microscope (OM) from Carl Zeiss Axio Scope.A1 and a Quanta 400 FEI scanning electron microscope equipped with Oxford energy dispersive X-ray spectroscopy (EDX) were employed for the microscopic analysis. The metallographic samples were ground using a series of silicon carbide papers and a suspension of 3 µm alumina. To reveal the microstructures, a solution consisting of 2% nitric acid and 98% ethanol, known as the 2% initial solution, was employed for etching all of the samples.

2.3. Microhardness Testing

The MMT-X7B model micro-Vickers hardness tester, made in Japan by Matsuzawa Company, was used to collect the measurements over a cross-section of the welded rail sample at various locations, such as the weld metal, HAZ, and base rail. Under 2 mm from the top surface, the micro-Vickers hardness of the samples was measured. Loads of 200 g (HV0.2) and 10 seconds dwell time were used to capture the hardness profiles at intervals of 0.5 mm.

2.4. Measuring the interlamellar spacing of pearlite

The interlamellar spacings of pearlite were measured on SEM images using Image J software. The interlamellar spacing of pearlite from the base Rail steel, thermite weld metal, HAZ of FCAW 1, and HAZ of FCAW 2 was measured and the obtained results were compared.

3. RESULTS AND DISCUSSION

3.1. Optical Microscopy (Macro and Microstructure)

The macro and microstructures of FCAW 1 and FCAW 2 as captured by an optical microscope are depicted in **Figures 3** and **4**. In **Figures 3** and **4**, the macrographs show a variety of locations (including the HAZ and the weld metal from thermite and FCAW) and confirm that no cracks and defects were present in the cross-sectional welded sample. The HAZ sizes of FCAW were measured at 2 mm from the top surface of the railhead, and they averaged around 5 mm on both sides. It can be observed in the macrographs that the FCAW weld metal and HAZ appeared between the boundary of the thermite weld and the base rail. This also indicates that both thermite weld metal and base rail steel were unaffected by the FCAW process. The location of specific microstructures is shown on their corresponding macrographs of FCAW 1 and FCAW 2 (see **Figures 3** and **4**). In both conditions, the microstructures of thermite weld and its HAZs exhibit pearlite microstructures with pro eutectoid ferrite. Near the base rail, where the HAZ of the thermite ends, spherodized pearlite microstructure is shown. Because of its altered microstructure, this region of thermite weld is rather soft. The main purpose of this research is to improve this specific area using the FCAW process.

Thermite-welded samples can be analyzed by examining five main locations. The regions for investigation include weld metal (WM), the coarse-grain HAZ (CGHAZ), the fine-grain HAZ (FGHAZ), intercritical HAZ (ICHAZ), and the base rail (Burapa *et al*., 2024). In both conditions, the microstructure of the thermite weld and its HAZs is similar. The thermite weld metal microstructure shows pearlitic microstructure with larger grain and some pro-eutectoid ferrite. The HAZs of thermite welded rail consist of three distinct zones. The HAZ adjacent to the thermite weld metal exhibits a pearlitic microstructure with a larger grain size, but smaller than that of the weld metal. The grain size of the CGHAZ is larger in comparison to the grain

DOI: https://doi.org/10.17509/ijost.v9i2.71238
p-ISSN 2528-1410 e-ISSN 2527-8045

size of the FGHAZ and ICHAZ. Within CGHAZ and ICHAZ, the pearlitic FGHAZ was identified. The ICHAZ was observed at the boundary of HAZ adjacent to the base rail steel. The R260 rail was utilized as the base material for both conditions. The microstructure of the R260 rail is composed of a fully pearlitic structure. Pearlitic microstructure with fine grain is shown in the HAZs of FCAW in both conditions. Pearlite microstructure is influenced by its interlamellar spacing. However, under an optical microscope, pearlite's interlamellar spacing is not visible. The microstructures of FCAW weld metals exhibit variations under different conditions. In the case of FCAW 1, the weld metal's microstructure is bainite, whereas the weld metal microstructure in FCAW 2 is entirely acicular ferrite. It can be noted that varying heat inputs and preheating temperatures altered the FCAW weld microstructure.

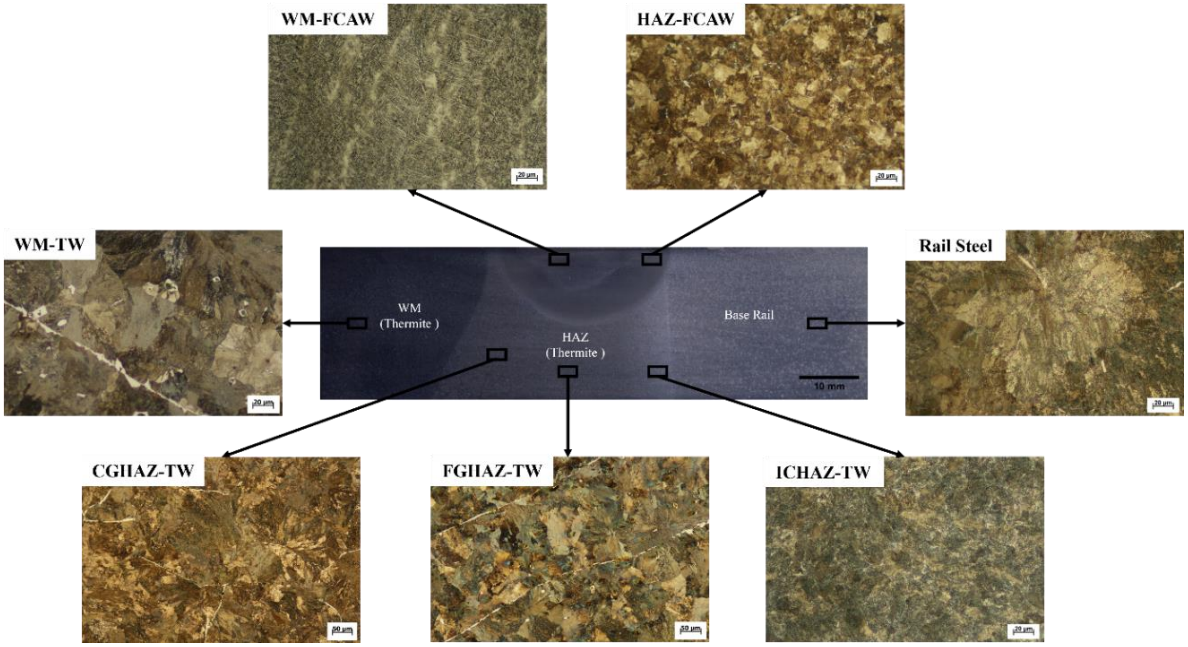

Figure 3. Macro and microstructure (Optical) of FCAW 1.

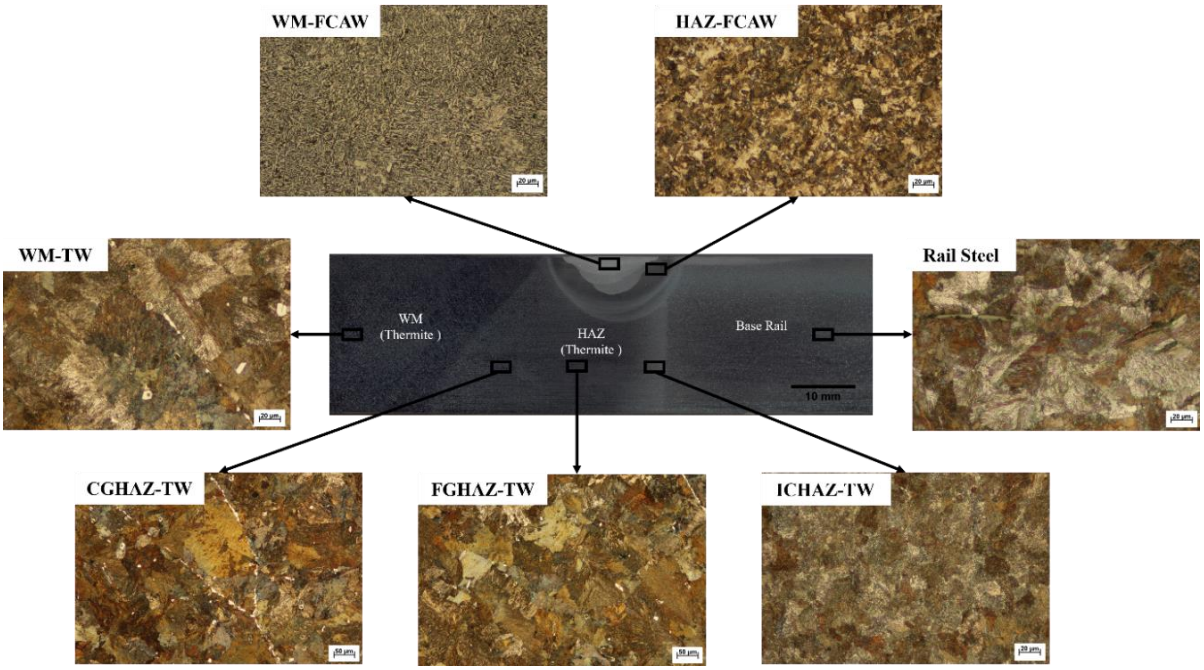

Figure 4. Macro and microstructure (Optical) of FCAW 2.

DOI: https://doi.org/10.17509/ijost.v9i2.71238
p- ISSN 2528-1410 e- ISSN 2527-8045

3.2. Scanning Electron Microscopy (SEM)

SEM images of pearlitic rail steel (R260) under different magnifications are displayed in **Figure 5**. The SEM micrograph in **Figure 5 (a)** shows cementite as white and ferrite as black. The color of pearlite microstructure revealed in SEM images differs from light micrographs. When observed at high magnification, the lamellar eutectoid structure of pearlite becomes visible in an electron microscopic image with greater resolution, as shown in **Figure 5b**. The pearlite structure can be identified by its presence of a parallel nanoscale lamella structure composed of ferrite and cementite. The formation of this structure originates from the isothermal decomposition of austenite at around 723°C. Carbon steel containing a pearlitic microstructure is commonly employed as the primary material for rail steel. The lamellar microstructure referred to as pearlite consists of aligned cementite lamellae embedded inside a softer ferrite matrix. The pearlitic rail steel exhibits higher wear resistance and strength. The mechanical properties of this microstructure are well-suited for utilization in the railway (Nikas *et al*., 2017; Masoumi *et al.*, 2019).

In **Figure 6**, the SEM micrographs of thermite weld metal with different magnifications are shown. The microstructure of thermite weld metal exhibits a lamellar pearlite structure. When comparing the base rail steel, it is observed that the pro eutectoid ferrite phase exhibits scattering within the pearlitic microstructure in the thermite weld metal, as shown in **Figure 6a**. Since the process of thermite welding can be considered a form of casting, it was anticipated that the weld metal microstructure would mostly exhibit elongated and coarse grains that are oriented along the direction of heat transfer. The occurrence of pro eutectoid ferrite formation in the weld metal microstructures can be attributed to the interaction between the peak temperature and the rate of cooling. The interlamellar spacings of pearlite in the thermite weld metal are narrower than those of the base rail. **Figure 6b** shows the microstructure of thermite weld metal at higher magnification.

Figure 7 displays the SEM images revealing the spheroidization of pearlite at the ICHAZ of thermite weld metal under different magnifications. The images are taken at two different magnifications: 25,000X in **Figure 7a** and 50,000X in **Figure 7b**. Spherical cementite phases were observed under the SEM. The spheroidized microstructures exhibit an appearance of cementite in a spherical morphology, which is uniformly dispersed throughout a ferrite matrix. The spheroidization process typically takes place at the eutectoid temperature of 723°C (Fegredo *et al.*, 1993). Pearlite commonly has a lamellar morphology. The formation of a spheroidized microstructure results in reduced hardness, hence rendering the HAZ susceptible to weakening (Oo & Muangjunburee, 2023).

Figure 8 shows the SEM micrograph of FCAW weld metal under different conditions. The microstructure of FCAW weld metal varied depending on the welding conditions. Bainite microstructure is visible in the weld metal of FCAW 1 (**Figure 8a**), whereas acicular ferrite with metallic inclusions comprises the weld metal of FCAW 2 (**Figure 8b**). During the process of bainite formation, the ferrite phase transforms a lath morphology that is aligned with the austenite grain boundaries. In contrast to bainite, the formation of acicular ferrite occurs through nucleation on the surface of intragranular nonmetallic inclusions (Madariaga *et al.*, 2001). The initial acicular ferrite plates develop on the non-metallic inclusions, while the nucleation of secondary acicular ferrite takes place on the initially formed ferrite plates (Loder *et al.*, 2017).

DOI: https://doi.org/10.17509/ijost.v9i2.71238
p-ISSN 2528-1410 e-ISSN 2527-8045

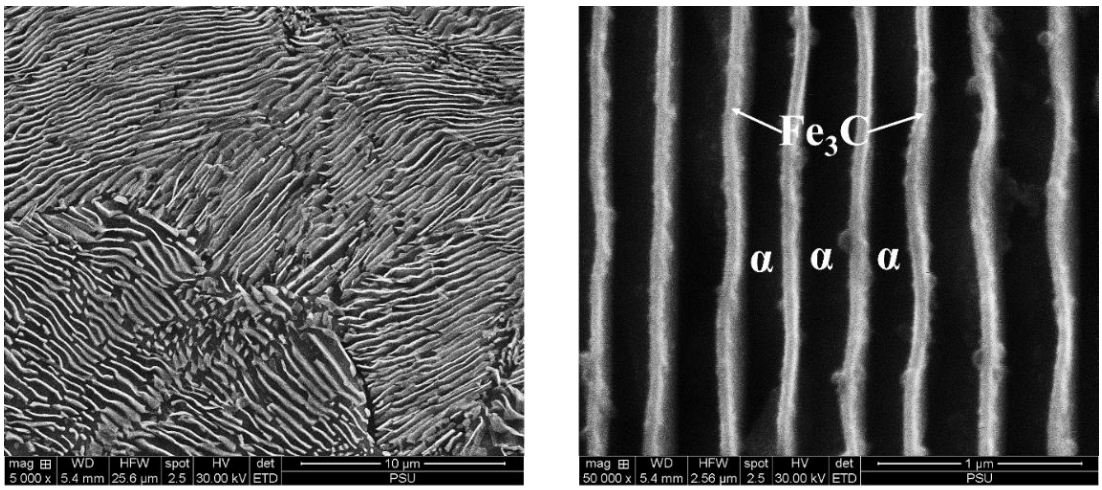

Figure 5. SEM micrographs of rail steel (a) 5,000 x magnification (b) 50,000 x magnification.

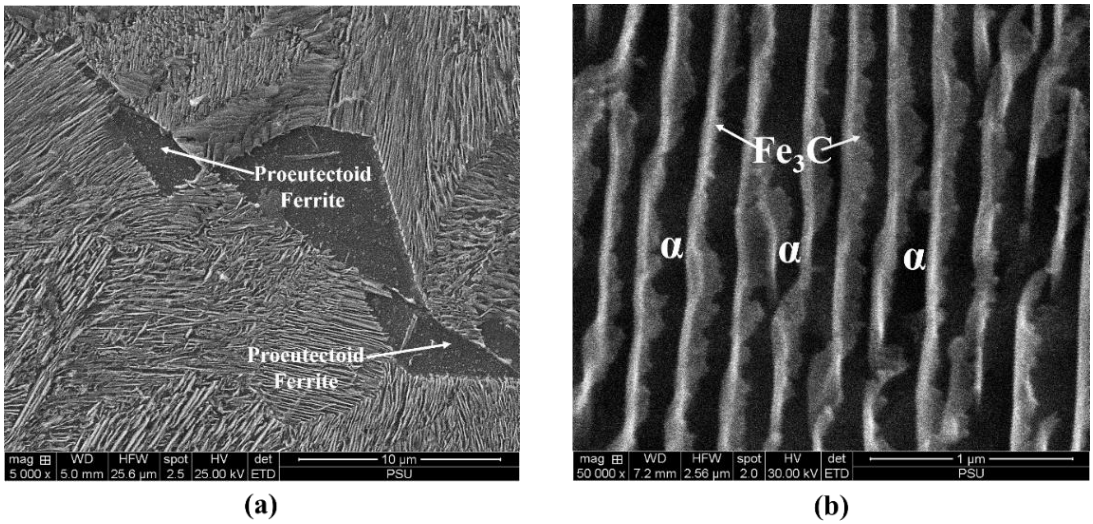

Figure 6. SEM micrographs of thermite weld metal (a) 5,000 x magnification (b) 50,000 x magnification.

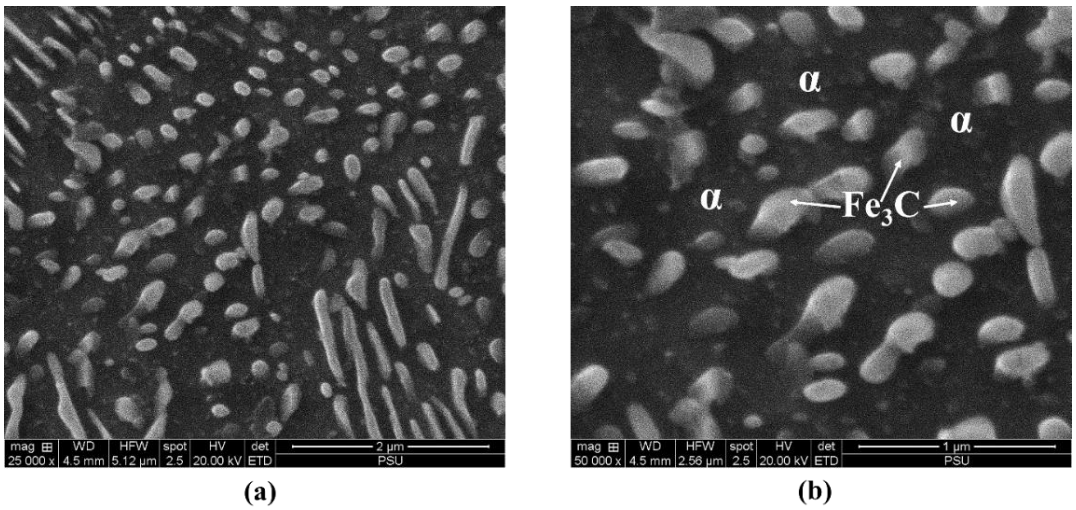

Figure 7. SEM micrographs of spheroidized cementite at intercritical HAZ of thermite weld (a) 25,000 x magnification (b) 50,000 x magnification.

DOI: https://doi.org/10.17509/ijost.v9i2.71238
p- ISSN 2528-1410 e- ISSN 2527-8045

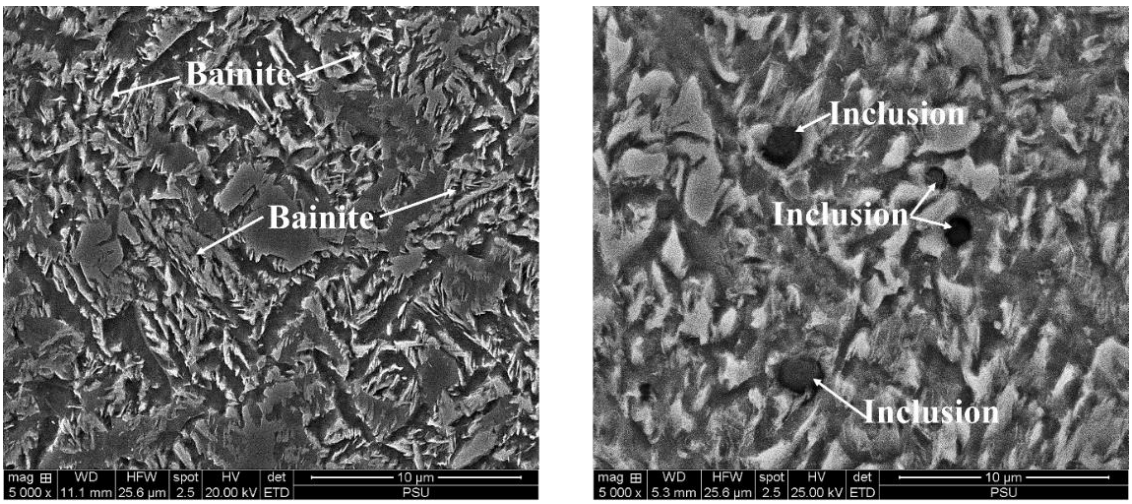

Figure 8. SEM micrographs of FCAW weld metal (a) FCAW 1 (b) FCAW 2.

The elemental microanalysis of FCAW 1 weld metal was conducted using EDX. The EDX spectra investigated on the SEM image of FCAW 1 weld metal are shown in **Figure 9**. The weld metal of FCAW 1 is mainly composed of iron (Fe), and small amounts of manganese (Mn), silicon (Si), and chromium (Cr) are also detected. Three locations were examined on the SEM image. The results of elemental spectra exhibited similarity across all points.

Figure 10 shows the SEM image of FCAW 2 weld metal and its EDX spectra. The main area of the EDX analysis in FCAW 2 weld metal was metallic inclusion. The detected components in the inclusion were determined to be a mixture consisting of titanium oxide and manganese sulfide. The EDX spectra show that the inclusion has a high concentration of oxygen, manganese, and titanium, and a low concentration of sulfur. The inclusion of titanium and manganese is important for the formation of acicular ferrite. Titanium can react with oxygen to generate various titanium oxides. These titanium oxides have been identified to have a high level of reactivity, particularly in serving as nucleation sites for the formation of acicular ferrite. The high content of manganese facilitates the incorporation of inclusions and promotes the initiation of acicular ferrite formation (Loder *et al.*, 2017). Specifically, the inclusion contains two different regions, characterized by various colors of grey and black. Based on the results of spectrum 1 at the grey area, high concentrations of manganese and titanium were observed. The results from spectrum 2 characterized at the black area exhibit somewhat lower levels of titanium and oxygen in comparison to the elemental analysis results of spectrum 1. It can be noted that the color of the inclusion is influenced by the concentration of titanium present inside it. The results of spectrum 3 and spectrum 4 show the comparable elemental composition results of FCAW 1.

The SEM microstructure of the HAZs for FCAW 1 is depicted in **Figure 11a** at a magnification of 10,000x and in **Figure 11b** at a magnification of 50,000x. **Figure 12a** and **Figure 12b** show the microscopic structures of the HAZs for FCAW 2 at 10,000X and 50,000X magnification, respectively. The lamellar pearlite microstructure has been revealed in both cases. The lamellar spacings of pearlite exhibited variations under different welding conditions. In the context of FCAW 1, the use of lower heat input and shorter preheating temperatures, in comparison to FCAW 2, led to an accelerated cooling rate. A more rapid cooling rate leads to the production of a finer lamellar spacing of pearlite due to the accelerated transition of austenite into pearlite. A reduced interlamellar spacing contributes to enhanced hardness in the steel (Modi *et al.*, 2001).

DOI: https://doi.org/10.17509/ijost.v9i2.71238
p-ISSN 2528-1410 e-ISSN 2527-8045

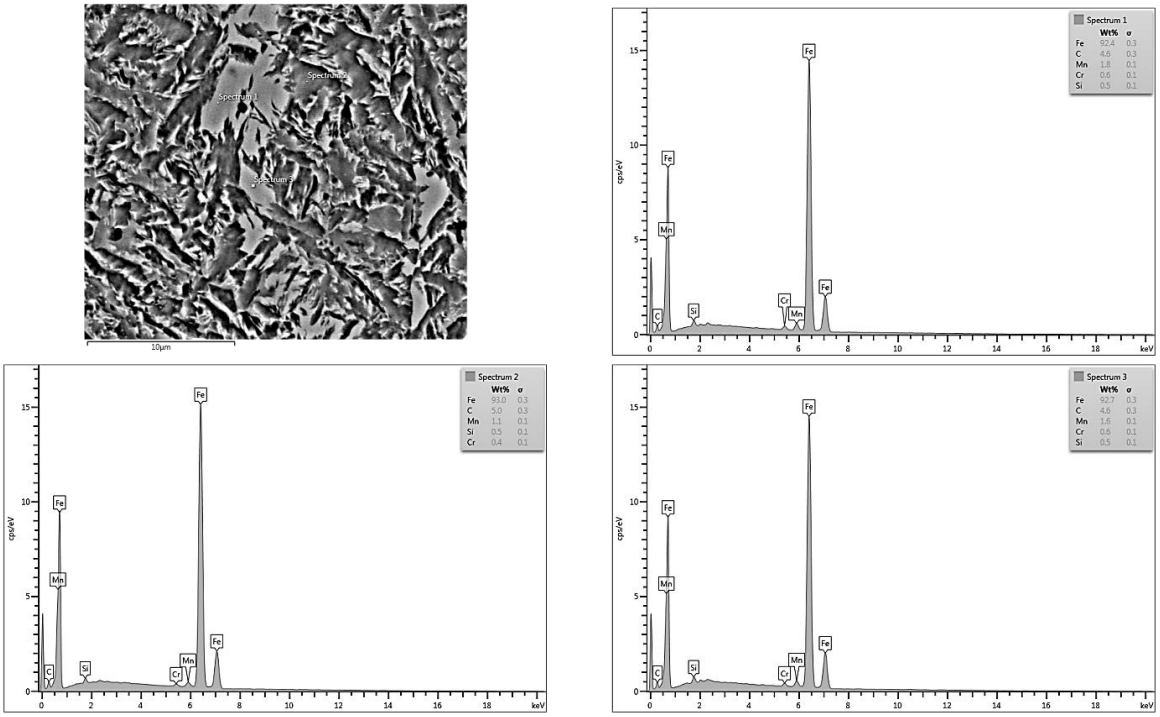

Figure 9. EDX elemental analysis on the SEM micrograph of FCAW 1 weld metal.

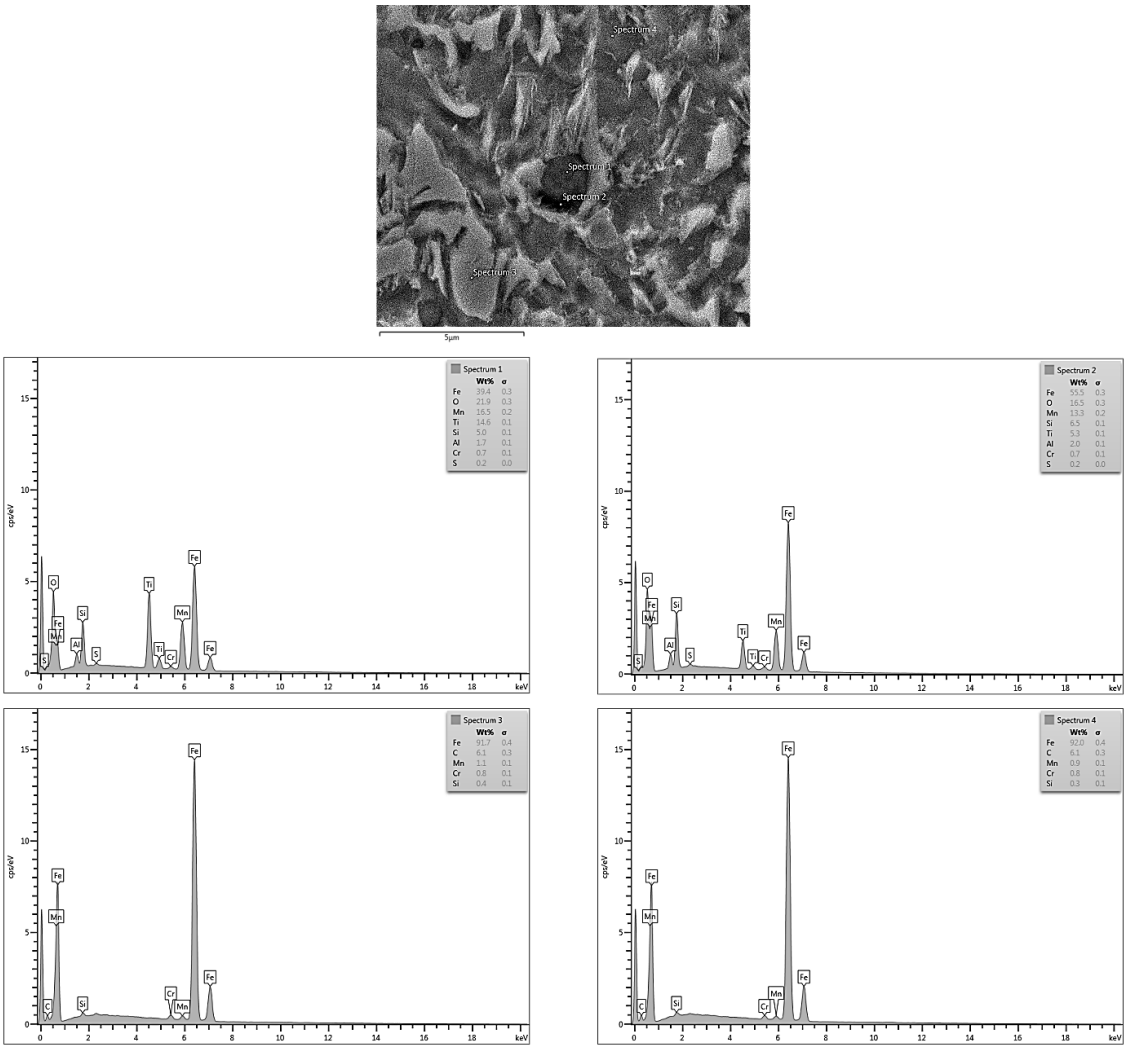

Figure 10. EDX elemental analysis on the SEM micrograph of FCAW 2 weld metal.

DOI: https://doi.org/10.17509/ijost.v9i2.71238
p- ISSN 2528-1410 e- ISSN 2527-8045

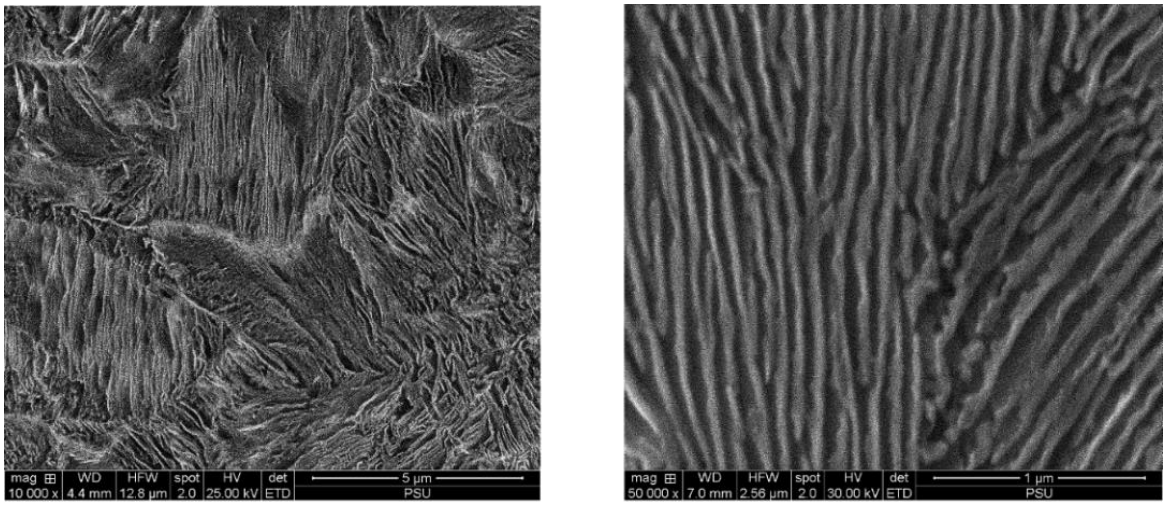

Figure 11. SEM micrographs of HAZ of FCAW 1 (a) 10,000 x magnification (b) 50,000 x magnification.

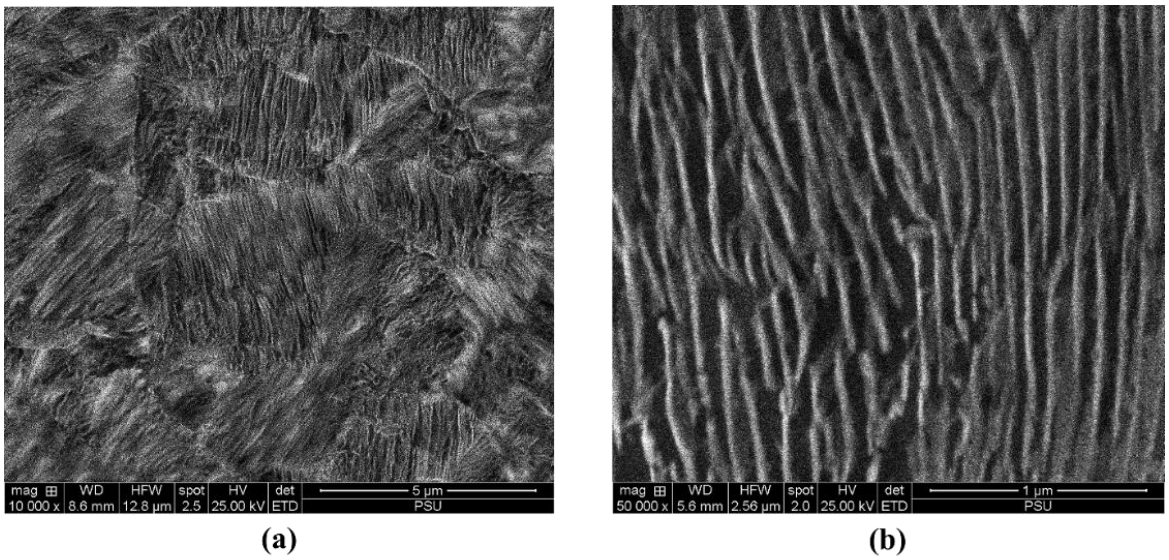

Figure 12. SEM micrographs of HAZ of FCAW 2 (a) 10,000 x magnification (b) 50,000 x magnification.

3.3. Hardness

Figure 13 shows the hardness profiles of the normal thermite weld, FCAW 1, and FCAW 2 conditions across the thermite weld metal to base rail. These results were acquired at 2 mm from the top surface of the rail head. The heat generated by FCAW affected two regions located on the measurement line. These regions refer to the area close to the fusion line of the thermite weld and the area close to the end of the thermite HAZ near the base rail (see **Figure 13**). The hardness values of two HAZs of FCAW are found to be similar under both conditions. The main concern to improve in this study is at ICHAZ of thermite welded condition. This area's hardness is around 250 HV. After repairing the low hardness area at the ICHAZ of thermite weld with FCAW 1 condition, the hardness is around 410 HV. Conversely, when employing the FCAW 2 condition, the hardness is approximately 340 HV. When compared to the hardness of the original rail and thermit weld metal, the values obtained after repair using both FCAW conditions are higher. However, the hardness values of FCAW 2

DOI: https://doi.org/10.17509/ijost.v9i2.71238
p-ISSN 2528-1410 e-ISSN 2527-8045

(about 340 HV) are comparable to those of the original rail steel (about 300 HV) and thermite weld metal (about 320 HV). Compared to the original rails steel and thermite weld metal, FCAW 1 has much higher hardness values. The hardness of the weld metal by FCAW 2 is around 325 HV, while the hardness of the weld metal by FCAW 1 is around 385 HV. The identical alloyed commercial electrode was employed; however, variations in welding heat input and preheating temperature resulted in a difference of around 60 HV in the weld metal hardness. In both FCAW 1 and FCAW 2, the hardness of HAZ is higher than that of the weld metal. It can be noted that the microstructure is significantly important for evaluating the hardness.

3.4. Measuring the Interlamellar Spacing of Pearlite

Table 2 presents a comparison of the measured interlamellar spacing and average hardness values for the base rail, thermite weld metal, HAZ of FCAW 1, and HAZ of FCAW 2. The interlamellar spacings were determined using SEM images. The HAZs of FCAW are situated on the pearlitic rail steel and their microstructure shows lamellar pearlite. Moreover, the initial region of FCAW's HAZ is characterized as a spheroidized microstructure, where the hardness decreases. The interlamellar spacings of the base rail and normal thermite weld are around 230 nm and 180 nm. The interlamellar spacings of HAZ of FCAW 1 and FCAW 2 are around 80 nm and 105 nm, respectively. Based on the results, rail steel exhibited the broadest lamellar spacing, while the HAZ of FCAW 1 displayed the narrowest lamellar spacing.

Figure 14 illustrates how it affects interlamellar spacing on the hardness of pearlitic microstructures. The hardness of pearlite decreases as the interlamellar spacing becomes broader. The interlamellar spacing of rail steel exhibited the greatest width, while its average hardness demonstrated the lowest value in comparison to the other conditions. The present investigation revealed that the HAZ of FCAW 1 exhibited the shortest interlamellar spacing of pearlite and the maximum hardness. However, the hardness of FCAW 1 is not equivalent to that of rail steel and the original thermite weld metal. In contrast, the hardness of the HAZ in FCAW 2 is slightly greater than that observed in rail steel and thermite weld metal. A hardness level below 350 HV is accepted as appropriate for the restoration of pearlitic rail steel due to being comparable to its hardness.

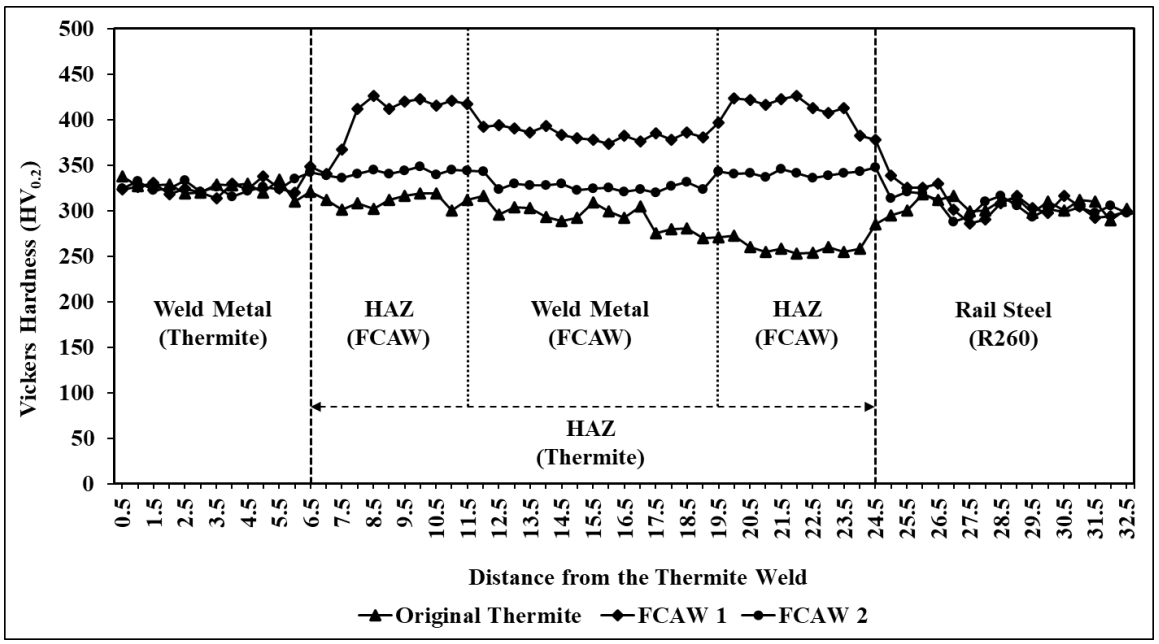

Figure 13. Hardness profiles along thermite weld metal to parent rail steel.

DOI: https://doi.org/10.17509/ijost.v9i2.71238
p-ISSN 2528-1410 e-ISSN 2527-8045

Table 2. Comparison between interlamellar spacing of pearlite and average hardness.

Techniques	Rail Steel	Thermite Weld	HAZ of FCAW 1	HAZ of FCAW 2
Interlamellar Spacing	226 ± 24 nm	186 ± 19 nm	79 ± 10 nm	102 ± 12 nm
Average Hardness	299 ± 18 HV	320 ± 10 HV	409 ± 16 HV	341 ± 3 HV

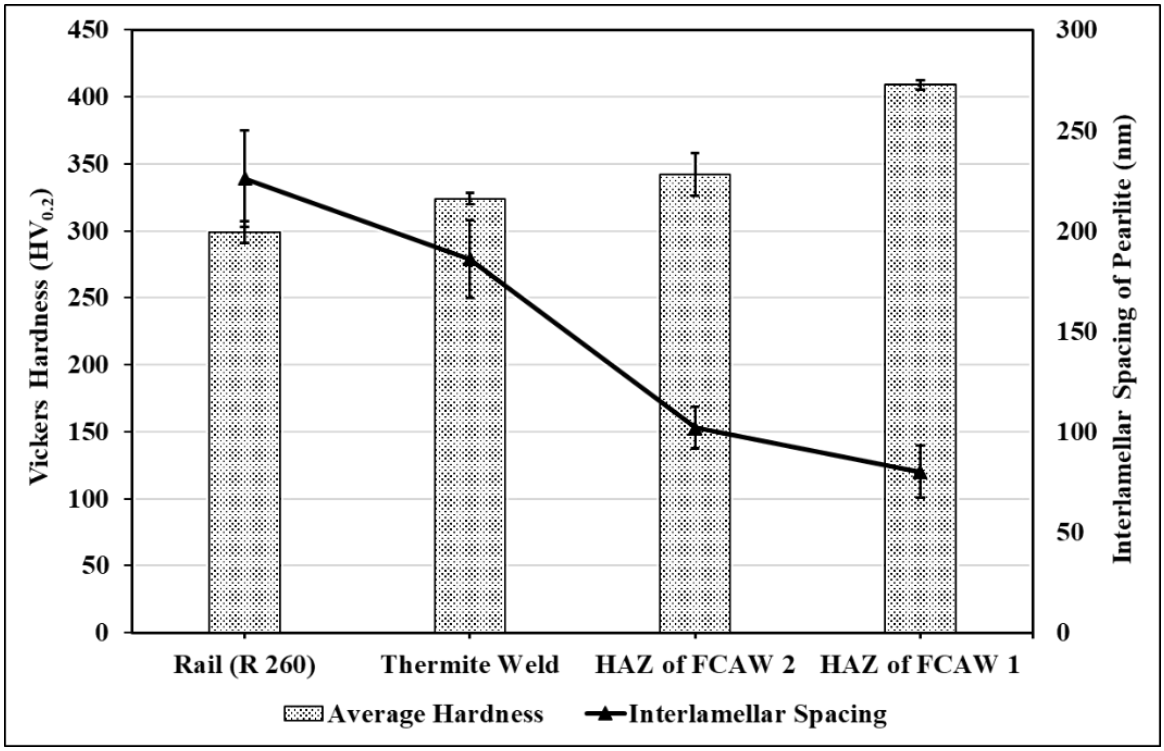

Figure 14. Comparison of average hardness and interlamellar spacing of pearlite.

3.5. Discussion

This research studied the effects of welding heat inputs and preheating temperatures of repair rail head surface by flux-cored arc welding at HAZ of thermite welded rail. Welding heat input and preheating temperature affected the cooling rate of weld metal and its HAZs. The cooling rate influenced the microstructure and hardness of the repair weld. The two different welding currents and preheating temperature which influenced the cooling rate were applied and compared for the best options.

The optimum size for the HAZ of thermite on the surface of the rail is around 18-20 mm. The specific design of the slot located within the range of the HAZ surface is critical for this study. The effect of the repair weld will not affect the quality of the initial thermite weld metal and the base rail steel. Consequently, the slot was positioned in the center of the HAZ, ensuring that all effects resulting from the FCAW were limited to the thermite HAZ boundaries. The thermal effect caused by FCAW resulted in the alteration of the lower hardness areas, leading to the re-austenitization of the spheroidized region within the HAZ of the thermite weld. This re-austenitization was primarily driven by the heat emerging from the FCAW welding process.

The heat generated during the FCAW process influenced both sizes of the slot. Due to the high temperatures produced by the FCAW process, the spheroidized microstructure refined into a fine pearlite microstructure. During the process of welding, the spheroidized cementite transforms austenite, resulting in the formation of a pearlite microstructure at the eutectoid temperature during cooling. The methodologies and results obtained from this study possess

DOI: https://doi.org/10.17509/ijost.v9i2.71238
p-ISSN 2528-1410 e-ISSN 2527-8045

the potential for direct implementation in practical engineering contexts within the railway industry, characterized by rapid implementation and cost-effectiveness.

Insufficient heat was observed to affect the ICHAZ areas near the unaffected rail during the process of thermite welding. The process of spheroidization is mostly influenced by the stage of partial austenitization and the faster cooling rate (Nishikawa & Goldenstein, 2019; Ankit *et al.*, 2015). As a consequence, the lamella pearlite structure undergoes a transformation wherein sphere-shaped cementite forms on the ferrite matrix. Due to this process, the HAZs created during thermite welding are substantially softer than the parent rail steel. The presence of a spheroidized cementite in the HAZ of thermite welded rail is considered a potential disadvantage of thermite rail welding due to its lower hardness. Therefore, these areas are necessary to improve by a simple and cost-effective method.

FCAW is a highly efficient welding process that can be readily employed in railway construction and maintenance sites. The FCAW procedure is commonly employed to repair surface imperfections seen on conventional rail heads in practical applications. The FCAW method presents several advantages in comparison to alternative welding methods. These advantages involve superior deposition rates in comparison to gas metal arc welding (GMAW), enhanced ease of use and adaptability in comparison to submerged arc welding (SAW), and increased productivity when compared to shielded metal arc welding (SMAW) (Mohamat *et al*., 2012; Masoumi *et al.*, 2019). Moreover, FCAW combines the most advantageous settings of GMAW and SMAW to establish a remarkable welding procedure (Holly *et al.*, 2019).

The cooling rate is a significant factor in determining the final microstructure of weld metal and HAZs. The cooling rate is influenced by the preheating temperature and heat input. According to Aglan *et al.* (2013), a slower cooling rate is exhibited when the preheating temperature and heat input increase. The consideration of the cooling rate of steel from the austenitic stage is significant concerning the production of acicular ferrite. When subjected to the same alloying, a faster cooling rate has the potential to result in the formation of bainite nucleated at the grain boundaries. Conversely, a slower cooling rate is more likely to the formation of acicular ferrite nucleated at the non-metallic inclusions (Abson, 2018). As a result, the weld metal of FCAW 1 showed a bainitic microstructure, while the weld metal microstructure of FCAW 2 revealed acicular ferrite phases.

Khan *et al*. (2019) observed that a higher cooling rate leads to a reduction in the interlamellar spacing of pearlite. The interlamellar spacing in pearlite microstructure, where the distance between two lamellae of cementite is a significant variable in determining the hardness of pearlite. In a study published by Porcaro *et al*. (2019), pearlite exhibiting narrower interlamellar spacings exhibited greater values of hardness. The hardness of pearlitic steel increases when the interlamellar spacing decreases. The interlamellar spacings of pearlite in the thermite weld metal are narrower than those of the base rail. Therefore, the hardness of thermite weld metal is a bit higher than that of rail steel.

According to the results of this study, the HAZ of FCAW 1 exhibited an interlamellar spacing of about 79 nm and a hardness value of approximately 409 HV. On the other hand, the HAZ of FCAW 2 revealed a hardness value of approximately 340 HV and an interlamellar spacing of approximately 100 nm. Additionally, Wu and Bhadeshia (2012) found that the pearlite with interlamellar spacing of 50 nm showed 422 HV. The obtained result from the following research demonstrates a similarity to the finest interlamellar spacing observed in pearlite at HAZ of FCAW 1, measuring approximately 79 nm, and the hardness of this region was found to be approximately 409 HV.

DOI: https://doi.org/10.17509/ijost.v9i2.71238
p- ISSN 2528-1410 e- ISSN 2527-8045

The hardness of the repaired weld metal and its HAZs are crucial factors to consider. **Table 3** provides the comparative studies of rail head repair under different rails and welding processes. In this research, the original rail steel has a hardness of approximately 300 HV, while the thermite weld metal demonstrates a hardness of approximately 320 HV. The repaired weld metal and its HAZs should not be more than 350 HV because the hardness of the repair weld should be comparable with the original thermite weld metal and base rail (Oo & Muangjunburee, 2024). Based on the results and discussion, it can be determined that the parameters of the FCAW 2 condition are the most suitable for repairing the thermite welded rail head.

Table 3. Comparison of different repair welding processes and hardness of repaired weld metal and HAZ.

References	Repaired Area	Rail Steel Grade	Base Rail Hardness	Repaired Methods	Repaired Weld	Repaired Weld Hardness	HAZ Hardness
Hernández *et al.* (2016)	Thermite Weld and its HAZs	Fully Pearlitic Rail	-	Laser Cladding	Pearlite	360 HBN	-
Allie *et al.* (2011a)	Rail Head Surface	Pearlitic Rail and Bainitic Rail	375 HBW and 420 HBW	GMAW	Ferrite	300 HBW	340 HBW and 400 HBW
Aglan *et al.* (2013)	Rail Head Surface	R260 Rail	360 HB	GMAW	Ferrite	313 HB	313 HB
SaifulAkmal and Wahab (2021)	Rail Head Surface	UIC-54 Rail	300 HV	FCAW	Acicular Ferrite	381 HV	350 HV
Jun *et al.* (2016)	Rail Head Surface	UIC60 Gr.260 Rail	310 HV	GMAW	Ferrite and Pearlite	320 HV	400 HV
Mat *et al.* (2015)	Rail Head Surface	RE115 Rail	377 HV	SMAW	Delta Ferrite	323 HV	419 HV
Mortazavian *et al.* (2020)	Rail Head Surface	880 C-Mn Rail	95 HRB	SAW	Ferrite, Pearlite and Austenite	80 HRB	92 HRB
Muangjunburee *et al.* (2023)	Rail Head Surface	BS 100A	330 HV	SMAW	Bainite	400HV and 450 HV	-
This study (FCAW 1)	HAZ of thermite weld surface	R260 Rail	300 HV	FCAW	Bainite	385 HV	410 HV
This study (FCAW 2)	HAZ of thermite weld surface	R 260 Rail	300 HV	FCAW	Acicular Ferrite	325 HV	340 HV

DOI: https://doi.org/10.17509/ijost.v9i2.71238
p-ISSN 2528-1410 e-ISSN 2527-8045

4. CONCLUSION

The subsequent conclusions can be clearly described:

(i) Despite using the same welding electrode, welding heat input and preheating temperature altered the weld metal microstructure. The weld metal has a bainite microstructure in FCAW 1 and acicular ferrite in FCAW 2. The hardness values depend on the microstructure. Bainitic weld metal from FCAW 1 is harder than that from FCAW 2. Weld metal hardness from FCAW 2 is 325 HV, while FCAW 1 is 385 HV, a difference of around 60 HV.

(ii) The HAZ of FCAW 1 and 2 exhibited fine pearlitic microstructure with varied interlamellar spacings. The rail steel exhibited the broadest lamellar spacing (226 ± 24 nm) and the smallest (79 ± 10 nm) in the HAZ (HAZ) of FCAW 1.

(iii) The hardness of the pearlitic microstructure depends on interlamellar spacing. The higher cooling rate reduced pearlite interlamellar spacing, resulting in a finer microstructure. Hardness increases with lamellar spacing decrease. HAZ hardness in FCAW 1 was 410 HV. This hardness is undesirable for pearlitic rail and thermite weld repairs in railway applications.

(iv) Slow cooling was maintained by increasing heat input and preheating temperature. In FCAW 2, HAZ and weld metal are comparable in hardness to rail steel and thermite weld metal.

(v) The current research summarizes that when it comes to repairing the damaged area of the thermite-welded rail head surface, it is highly recommended to use a high heat input and preheating temperature.

5. ACKNOWLEDGMENT

This research is funded by the National Science, Research and Innovation Fund (NSRF) and Prince of Songkla University (Grant No. ENG6601092S), as well as the Center of Excellence in Metals and Materials Engineering (CEMME) at Prince of Songkla University. The authors would like to acknowledge Mr. Wissarut Sangwiman, the Managing Director of Pearlite Construction Partnership (PCP) Company, Thailand, for his assistance in supporting the thermite welding performed out in this study. Also, the authors are grateful to Mr. Kanisorn Muangjunburee and Mr. Sittidet Yotsakun, who helped out with the FCAW welding experiments.

6. AUTHORS' NOTE

The authors declare that there is no conflict of interest regarding the publication of this article. The authors confirmed that the paper was free of plagiarism.

7. REFERENCES

Abson, D. J. (2018). Acicular ferrite and bainite in C–Mn and low-alloy steel arc weld metals. *Science and Technology of Welding and Joining*, *23*(8), 635-648.

Aglan, H. A., Ahmed, S., Prayakarao, K. R., and Fateh, M. (2013). Effect of preheating temperature on the mechanical and fracture properties of welded pearlitic rail steels. *Engineering*, *5*(11), 837.

Alhassan, M., and Bashiru, Y. (2021). Carbon equivalent fundamentals in evaluating the weldability of microalloy and low alloy steels. *World Journal of Engineering and Technology*, *9*(4), 782-792.

Allie, A., Aglan, H., and Fateh, M. (2011a). Fatigue crack growth of bainitic rail steel welds. *Science and Technology of Welding and Joining*, *16*(6), 535-540.

Allie, A., Aglan, H., and Fateh, M. (2011b). Microstructure-fracture behavior relationships of slot-welded rail steels. *Metallurgical and Materials Transactions A*, *42*, 2706-2715.

Ankit, K., Mukherjee, R., and Nestler, B. (2015). Deviations from cooperative growth mode during eutectoid transformation: Mechanisms of polycrystalline eutectoid evolution in Fe–C steels. *Acta Materialia*, *97*, 316-324.

Bonniot, T., Doquet, V., and Mai, S. H. (2018). Mixed mode II and III fatigue crack growth in a rail steel. *International Journal of Fatigue*, *115*, 42-52.

Burapa, R., Oo, H. Z., Sangwiman, W., and Muangjunburee, P. (2024). Influences of preheating parameters on the quality of weld by thermite rail welding. *Materials Research Express*, *11*(6), 066507.

Dahl, B., Mogard, B., Gretoft, B., and Ulander, B. (1995). Repair of rails on-site by welding. *Crossings*, *900*, 55-75.

Fegredo, D. M., Kalousek, J., and Shehata, M. T. (1993). The effect of progressive minor spheroidization on the dry-wear rates of a standard carbon and a Cr-Mo alloy rail steel. *Wear*, *161*(1-2), 29-40.

Grossoni, I., Hughes, P., Bezin, Y., Bevan, A., and Jaiswal, J. (2021). Observed failures at railway turnouts: Failure analysis, possible causes and links to current and future research. *Engineering Failure Analysis*, *119*, 104987.

Hauser, D. (1978). Welding of Railroad Rails-A Literature and Industry Survey. *Rail Steels-Developments, Processing and Use, ASTM Special Technical Publication*, *644*, 118-144.

Hernández, F. R., Okonkwo, A. O., Kadekar, V., Metz, T., and Badi, N. (2016). Laser cladding: The alternative for field thermite welds life extension. *Materials & Design*, *111*, 165-173.

Holly, S., Mayer, P., Bernhard, C., and Posch, G. (2019). Slag characterisation of 308L-type stainless steel rutile flux-cored wires. *Welding in the World*, *63*(2), 293-311.

Ilić, N., Jovanović, M. T., Todorović, M., Trtanj, M., and Šaponjić, P. (1999). Microstructural and mechanical characterization of postweld heat-treated thermite weld in rails. *Materials Characterization*, *43*(4), 243-250.

Jiang, W. J., Liu, C., He, C. G., Guo, J., Wang, W. J., and Liu, Q. Y. (2017). Investigation on impact wear and damage mechanism of railway rail weld joint and rail materials. *Wear*, *376*, 1938-1946.

Jun, H. K., Seo, J. W., Jeon, I. S., Lee, S. H., and Chang, Y. S. (2016). Fracture and fatigue crack growth analyses on a weld-repaired railway rail. *Engineering Failure Analysis*, *59*, 478-492.

DOI: https://doi.org/10.17509/ijost.v9i2.71238
p-ISSN 2528-1410 e-ISSN 2527-8045

Kendall, O., Fasihi, P., Abrahams, R., Paradowska, A., Reid, M., Lai, Q., Qiu, C., Mutton, P., Soodi, M., and Yan, W. (2022). Application of a new alloy and post processing procedures for laser cladding repairs on hypereutectoid rail components. *Materials*, *15*(15), 5447.

Kewalramani, R. G., Riehl, I., Hantusch, J., and Fieback, T. (2023). Numerical investigation of the cooling stage during aluminothermic welding of rails: Rapid welding process without preheating. *Thermal Science and Engineering Progress*, *37*, 101610.

Khan, A. R., Yu, S., Wang, H., and Jiang, Y. (2019). Effect of cooling rate on microstructure and mechanical properties in the CGHAZ of electroslag welded pearlitic rail steel. *Metals*, *9*(7), 742.

Kozyrev, N. A., Shevchenko, R. A., Usol'tsev, A. A., Prudnikov, A. N., and Bashchenko, L. P. (2020). Development and modeling of differentially heat-strengthened rail welding: welding and local heat treatment modeling. *Steel in Translation*, *50*, 139-145.

Lesage, T., Avettand-Fènoël, M. N., Masquelier, M., Danoix, F., and Kamgaing, L. (2023). Consequences of thermite welding on the microstructure of the heat-affected zone of a carbide-free bainitic steel rail. *Journal of Manufacturing Processes*, *108*, 746–763.

Li, W., Xiao, G., Wen, Z., Xiao, X., and Jin, X. (2011). Plastic deformation of curved rail at rail weld caused by train–track dynamic interaction. *Wear*, *271*(1-2), 311-318.

Liu, Y., Tsang, K. S., Zhi'En, E. T., Subramaniam, N. A., and Pang, J. H. L. (2021). Investigation on material characteristics and fatigue crack behavior of thermite welded rail joint. *Construction and Building Materials*, *276*, 122249.

Loder, D., Michelic, S. K., and Bernhard, C. (2017). Acicular ferrite formation and its influencing factors—A review. *Journal of Materials Science Research*, *6*(1), 24-43.

Madariaga, I., Gutierrez, I., and Bhadeshia, H. K. D. H. (2001). Acicular ferrite morphologies in a medium-carbon microalloyed steel. *Metallurgical and Materials Transactions A*, *32*, 2187-2197.

Masoumi, M., Echeverri, E. A. A., Tschiptschin, A. P., and Goldenstein, H. (2019). Improvement of wear resistance in a pearlitic rail steel via quenching and partitioning processing. *Scientific Reports*, *9*(1), 7454.

Mat, M. F., Musah, A. F., Tham, A. G., and Sulaiman, S. A. (2015). Evaluation of Rail Head Surface Repair Using SMAW Process with Pre Heating Condition. *Jurnal Teknologi (Science and Engineering)*, *76*(6), 79-83.

Merıç, C., Atık, E., and Şahın, S. (2002). Mechanical and metallurgical properties of welding zone in rail welded via thermite process. *Science and Technology of Welding and Joining*, *7*(3), 172-176.

Modi, O. P., Desmukh, N., Mondal, D. P., Jha, A. K., Yegneswaran, A. H., and Khaira, H. K. (2001). Effect of interlamellar spacing on the mechanical properties of 0.65% C steel. *Materials Characterization*, *46*(5), 347-352.

Mohamat, S. A., Ibrahim, I. A., Amir, A., and Ghalib, A. (2012). The effect of flux core arc welding (FCAW) processes on different parameters. *Procedia Engineering*, *41*, 1497-1501.

DOI: https://doi.org/10.17509/ijost.v9i2.71238
p-ISSN 2528-1410 e-ISSN 2527-8045

Mortazavian, E., Wang, Z., and Teng, H. (2020). Repair of light rail track through restoration of the worn part of the railhead using submerged arc welding process. *The International Journal of Advanced Manufacturing Technology*, *107*, 3315-3332.

Muangjunburee, P., Poolsiri, N., Chaideesungnoen, S., Naultem, A., Oo, H. Z., and Kongpuang, M. (2023). XRD observation on the weld metal of resurfaced rail steel. *Chiang Mai Journal of Science*, *50*(4), 1–11.

Mutton, P. J., and Alvarez, E. F. (2004). Failure modes in aluminothermic rail welds under high axle load conditions. *Engineering Failure Analysis*, *11*(2), 151-166.

Nikas, D., Meyer, K. A., and Ahlström, J. (2017). Characterization of deformed pearlitic rail steel. *IOP Conference Series: Materials Science and Engineering,* 219(1), 012035.

Nishikawa, L. P., and Goldenstein, H. (2019). Divorced eutectoid on heat-affected zone of welded pearlitic rails. *Jom*, *71*(2), 815-823.

Oo, H. Z., and Muangjunburee, P. (2023). Improving microstructure and hardness of softening area at HAZ of thermite welding on rail running surface. *Materials Today Communications*, *34*, 105485.

Oo, H. Z., and Muangjunburee, P. (2024). Hardfacing of thermite welded rail by flux-cored arc welding. *Wear*, *546–547*, 205314.

Porcaro, R. R., Faria, G. L., Godefroid, L. B., Apolonio, G. R., Cândido, L. C., and Pinto, E. S. (2019). Microstructure and mechanical properties of a flash butt welded pearlitic rail. *Journal of Materials Processing Technology*, *270*, 20-27.

SaifulAkmal, M. N., and Wahab, M. N. (2021). Characterization of UIC-54 rail head surface welded by hardfacing using flux-cored steel wire. *Recent Trends in Manufacturing and Materials Towards Industry 4.0: Selected Articles from iM3F 2020, Malaysia*, *2021*, 763-775.

Saita, K., Karimine, K., Ueda, M., Iwano, K., Yamamoto, T., and Hiroguchi, K. (2013). Trends in rail welding technologies and our future approach. *Nippon Steel & Sumitomo Metal Technical Report*, *105*, 84-92.

Schroeder, L. C., and Poirier, D. R. (1984). The mechanical properties of thermite welds in premium alloy rails. *Materials Science and Engineering*, *63*(1), 1-21.

Skyttebol, A., Josefson, B. L., and Ringsberg, J. W. (2005). Fatigue crack growth in a welded rail under the influence of residual stresses. *Engineering Fracture Mechanics*, *72*(2), 271-285.

Su, H., Li, J., Lai, Q., Pun, C. L., Mutton, P., Kan, Q., Kang, G., and Yan, W. (2020). Ratcheting behaviour of flash butt welds in heat-treated hypereutectoid steel rails under uniaxial and biaxial cyclic loadings. *International Journal of Mechanical Sciences*, *176*, 105539.

Tressia, G., Sinatora, A., Goldenstein, H., and Masoumi, M. (2020). Improvement in the wear resistance of a hypereutectoid rail via heat treatment. *Wear*, *442*, 203122.

Weingrill, L., Nasiri, M. B., and Enzinger, N. (2019). Thermo-metallurgically coupled numerical simulation and validation of multi-layer gas metal arc welding of high strength pearlitic rails. *Welding in the World*, *63*, 63-73.

DOI: https://doi.org/10.17509/ijost.v9i2.71238
p-ISSN 2528-1410 e-ISSN 2527-8045

Wu, K. M., and Bhadeshia, H. K. D. H. (2012). Extremely fine pearlite by continuous cooling transformation. *Scripta Materialia*, *67*(1), 53-56.

Yuan, X. Y., Zhan, C. B., Jin, H. B., and Chen, K. X. (2010). Novel method of thermite welding. *Science and Technology of Welding and Joining*, 15(1), 54-58.

DOI: https://doi.org/10.17509/ijost.v9i2.71238
p- ISSN 2528-1410 e- ISSN 2527-8045